Journal of Medical Imaging

MedicalImaging.SPIEDigitalLibrary.org

Automatic basal slice detection for cardiac analysis

Mahsa Paknezhad
Stephanie Marchesseau
Michael S. Brown

SPIE.

Mahsa Paknezhad, Stephanie Marchesseau, Michael S. Brown, "Automatic basal slice detection for cardiac analysis," *J. Med. Imag.* **3**(3), 034004 (2016), doi: 10.1117/1.JMI.3.3.034004.

Automatic basal slice detection for cardiac analysis

Mahsa Paknezhad,[a,*] Stephanie Marchesseau,[b] and Michael S. Brown[c]
[a]National University of Singapore, School of Computing, Department of Computer Science, Media Research Lab 4, AS6, Computing 1, 13 Computing Drive, 117417, Singapore
[b]A*STAR-NUS Clinical Imaging Research Centre, Centre for Translational Medicine (MD6), 14 Medical Drive, #B1-01, 117599, Singapore
[c]York University, Lassonde School of Engineering, Department of Electrical Engineering and Computer Science, 4700 Keele Street, Toronto, Ontario M3J 1P3, Canada

Abstract. Identification of the basal slice in cardiac imaging is a key step to measuring the ejection fraction of the left ventricle. Despite all the effort placed on automatic cardiac segmentation, basal slice identification is routinely performed manually. Manual identification, however, suffers from high interobserver variability. As a result, an automatic algorithm for basal slice identification is required. Guidelines published in 2013 identify the basal slice based on the percentage of myocardium surrounding the blood cavity in the short-axis view. Existing methods, however, assume that the basal slice is the first short-axis view slice below the mitral valve and are consequently at times identifying the incorrect short-axis slice. Correct identification of the basal slice under the Society for Cardiovascular Magnetic Resonance guidelines is challenging due to the poor image quality and blood movement during image acquisition. This paper proposes an automatic tool that utilizes the two-chamber view to determine the basal slice while following the guidelines. To this end, an active shape model is trained to segment the two-chamber view and create temporal binary profiles from which the basal slice is identified. From the 51 tested cases, our method obtains 92% and 84% accurate basal slice detection for the end-systole and the end-diastole, respectively. [DOI: 10.1117/1.JMI.3.3.034004]

Keywords: basal slice selection; long-axis view; two-chamber view; active shape model; cardiac; MRI.

Paper 16076PRR received May 12, 2016; accepted for publication Aug. 29, 2016; published online Sep. 20, 2016.

1 Introduction

Cardiac magnetic resonance (CMR) imaging is routinely used to evaluate cardiac function. CMR imaging consists of a time series of 12 to 15 short-axis view slices together with two long-axis views, a two-chamber view and a four-chamber view that are captured first to plan the short-axis view acquisition. One of the key applications of CMR is to measure the ejection fraction (EF) of the heart by estimating the volume of the left ventricle (LV) at the end-systolic and the end-diastolic phases. To compute the volume, most prior work focuses primarily on segmenting the short-axis view slices. The work done by Tufvesson et al.,[1] Ayed et al.,[2] and Jolly et al.[3] are typical examples. Several short-axis view segmentation methods have been compared by Petitjean and Dacher.[4] There are also challenges on LV volume reconstruction.[5]

Although significant progress has been made in automatic volume segmentation, to accurately estimate the EF, the basal slice at the end-systolic and end-diastolic phases needs to be specified. Errors in manual basal slice selection are the main cause of interobserver variability and can increase or decrease the EF by up to 6% and the ED volume by up to 21 ml.[6,7] Efforts have been made to automatically detect the base of the LV. Mahapatra,[8] e.g., proposed a learning-based method that trains a random forest classifier by extracting intensity, texture, and contextual features from a bounding box around the annotated points at both sides of the mitral valve. Lu and Jolly[9] proposed a learning-based method by introducing auxiliary markers along with contextual landmarks in the images to help identify the mitral value points. These methods work under the assumption that the basal slice is the first short-axis view slice below the line connecting the mitral valve points. However, the Society for Cardiovascular Magnetic Resonance (SCMR) recently published guidelines for cardiac image analysis[10] that describe precisely how to select the basal slice. According to the SCMR guidelines, the basal slice is the topmost short-axis view slice that has more than 50% myocardium around the blood cavity. Figures 1(a) and 1(b) show examples of short-axis view slices in which less than 50% myocardium and more than 50% myocardium is found around the blood cavity, respectively. Figures 1(c) and 1(d) show a heart for which the basal slice is not below the line connecting the mitral valve points.

While clinical guidelines describe basal slice detection based on features present in the short-axis view images, the base of the LV is visually clearer in the long-axis views of the heart. This is mainly because the base is primarily composed of moving blood which deteriorates quality of the acquired short-axis view slices in this area. As such, we focused our attention on the long-axis view of the LV for basal slice detection. Our proposed method utilizes the two-chamber view sequence together with the short-axis view slice planes. To the best of our knowledge, our work is the first to attempt automatic basal slice detection while exploiting the availability of the two-chamber view. For that purpose, we need to segment the LV in the two-chamber view. Segmentation of the myocardium wall from the two-chamber view allows us to estimate the thickness of the two opposite walls of LV where the short-axis view slice intersects the LV. These two pieces of data can be used to estimate whether more or less than 50% of the blood cavity is surrounded by myocardium for a certain short-axis view slice plane. The deployed

*Address all correspondence to: Mahsa Paknezhad, E-mail: mahsa@u.nus.edu

2329-4302/2016/$25.00 © 2016 SPIE

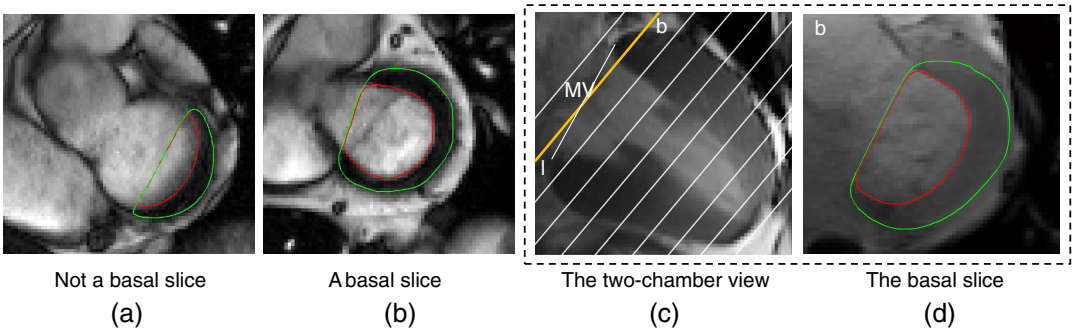

Fig. 1 (a) A slice with less than 50% myocardium around the blood cavity. (b) A slice with more than 50% myocardium. (c, d) An example of a heart for which the basal slice at end-systole is not below the line connecting the mitral valve points (l).

segmentation method needs to be automatic and relatively fast to provide segmentation of all the temporal images in a reasonable amount of time. Uzumcu et al.[11] have proposed using an active appearance model (AAM) to segment the long-axis view of the heart. Their method requires annotation of points on the heart as well as knowledge of the end-systolic and end-diastolic phases. Works by Zhuang et al.[12] and Van Assen et al.[13] leverage three-dimensional (3-D) heart models to help segment the LV from different orientations, including the two-chamber view. These approaches require significantly more training data compared to two-dimensional (2-D) models and involve a much longer run-time. In this paper, we have utilized a 2-D active shape model (ASM)[14] to automatically segment the two-chamber view of heart. Although we used an ASM for segmentation of the LV in the long-axis view, any of the mentioned methods could be automated (if not) and deployed. The main contribution in this paper, however, is how to use the segmentation results to find the basal slice at the end-systolic and end-diastolic phases of the cardiac cycle.

The paper is structured as follows: Sec. 2.1 demonstrates how the LV walls are segmented from the two-chamber view using an ASM of the LV. From the segmented LV in the two-chamber view images, the end-systolic and end-diastolic phases are estimated in Sec. 2.2 and the basal slice is identified in the short-axis view image in Sec. 2.3. Section 3 provides details about the experiments and demonstrates the effectiveness of the approach. This is followed by a discussion in Sec. 4 and a conclusion in Sec. 5.

2 Proposed Algorithm

In the following, we will explain how a 2-D model is trained and used for segmentation of the LV from the two-chamber view of the heart.

2.1 *Two-Chamber View Segmentation*

In order to segment the LV, an ASM[14] is used. ASM is a well-established method in the medical imaging and computer vision

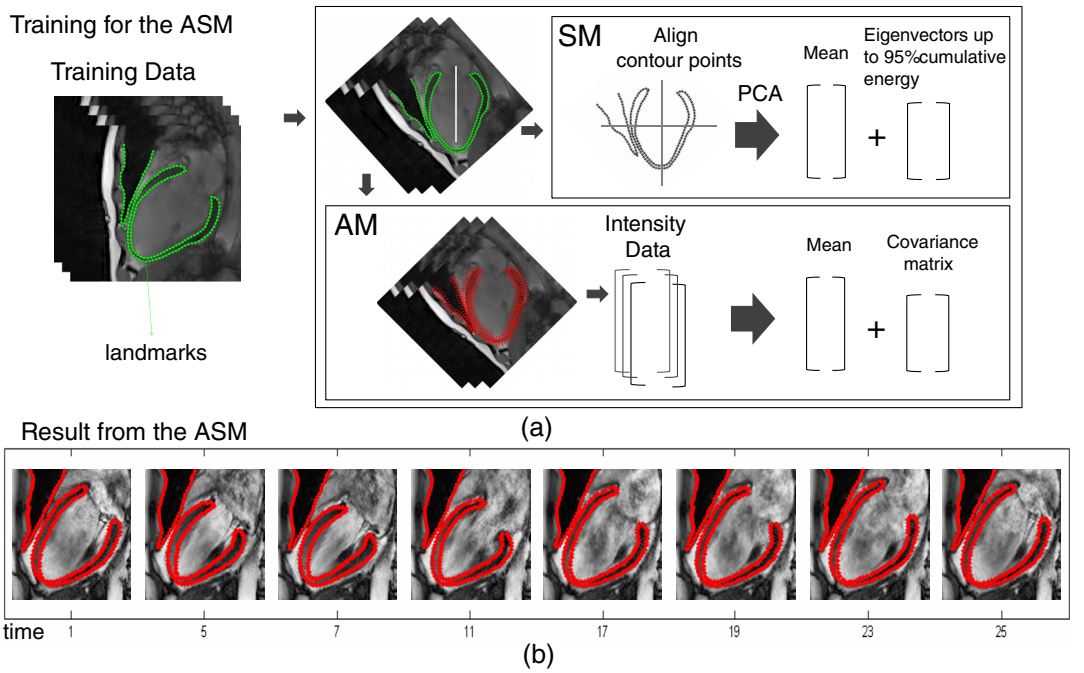

Fig. 2 (a) The training phase of the ASM and overall ASM information. (b) Model used to segment an input sequence.

community for segmentation. Training of the ASM requires the input of a number of landmarks on the contour of the object to be modeled. In the proposed implementation, 181 landmarks are considered around the walls of the LV as well as the lungs beside the heart. The model is trained with 650 segmented images that include 13 phases of the cardiac cycle from 50 MRI scans. Due to the variation in heart orientation in CMR studies, the images are first aligned and reoriented such that the heart is in an upright position, using the intersection vector of the two-chamber view and the four-chamber view.

Figure 2 shows the training phase of the ASM as well as an image sequence segmented by the trained ASM. The trained ASM is then applied to the input two-chamber view image sequence. The images in the time-series are both fed to an algorithm that segments one image in the time series and takes the segmentation result as the initial position for the segmentation of the next image and another algorithm that segments each image independently. The segmentation with the best normalized cross correlation is selected for that image. The best location to initialize the trained ASM on the first image in the sequence is also found by applying the ASM with a few iterations on a number of locations along the intersection vector of the two-chamber view and the four-chamber view slices and choosing the location with the best normalized cross correlation. Figure 3 shows a diagram of this procedure.

Given the segmented two-chamber view images, a one-dimensional (1-D) binary profile of the LV is created by collecting the intensity values of the segmented two-chamber view slice along the intersecting line between the two-chamber view slice and the corresponding short-axis view slice plane over time and concatenating the collected pixel values based on their time order. Figure 4 shows this procedure. An example of the constructed 1-D binary profiles for 12 short-axis view slices passing through a segmented two-chamber view of a heart is also shown in Fig. 5. The next goal is to estimate the end-systolic and end-diastolic phases of the heart and find the basal slice for the two phases from these binary profiles.

2.2 *Estimation of the End-Diastolic and the End-Systolic Phases*

Guidelines[10] state that the LV end-systolic and end-diastolic phases are the time when the segmented short-axis view slices are at their smallest and largest LV blood volumes, respectively. In order to estimate these two phases, the area of the blood cavity was measured for all the phases from the two-chamber view. This is carried out by finding the convex hull of the landmarks after segmentation and subtracting off the area of the myocardium which is surrounded by those landmarks. The two phases with the largest and smallest areas for the blood volume cavity are chosen as the end-systole and end-diastole. Figure 6 shows the area of the blood cavity of a heart measured for each time phase within the cardiac cycle and the identified end-systolic and end-diastolic phases. Accuracy of this method was tested and is discussed later in Sec. 3. Having estimated the end-systole and end-diastole, a certain number of phases around the estimated end-systolic and end-diastolic phases are considered in the next step while searching for the basal slice from the temporal binary profiles.

2.3 *Basal Slice Selection*

Searching for the basal slice is first conducted for the end-diastole. The basal slice selection algorithm goes through the 1-D binary profiles for the short-axis view slices from the top to the bottom until it finds the basal slice for the corresponding

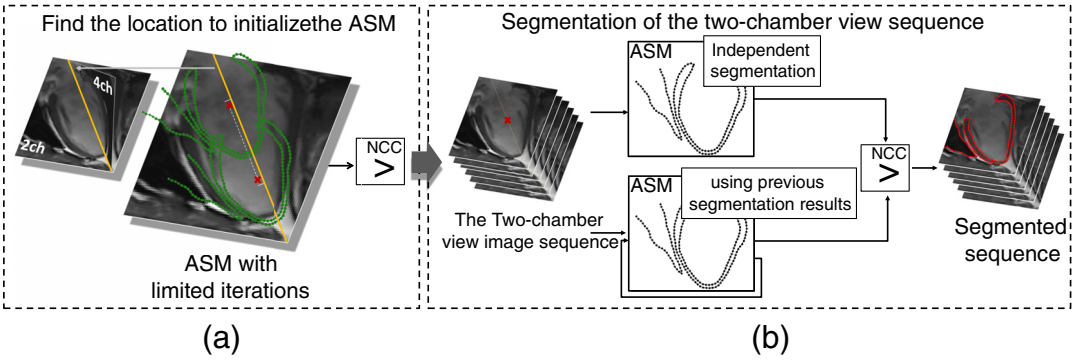

Fig. 3 (a) The location for initialization of the ASM on the image is found and (b) the best segmentation is chosen for each image in the sequence.

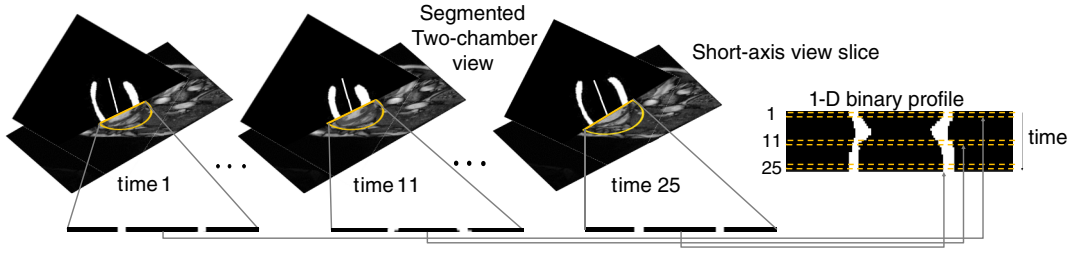

Fig. 4 The 1-D binary profile is constructed for a short-axis view slice, which passes through the segmented two-chamber view slice.

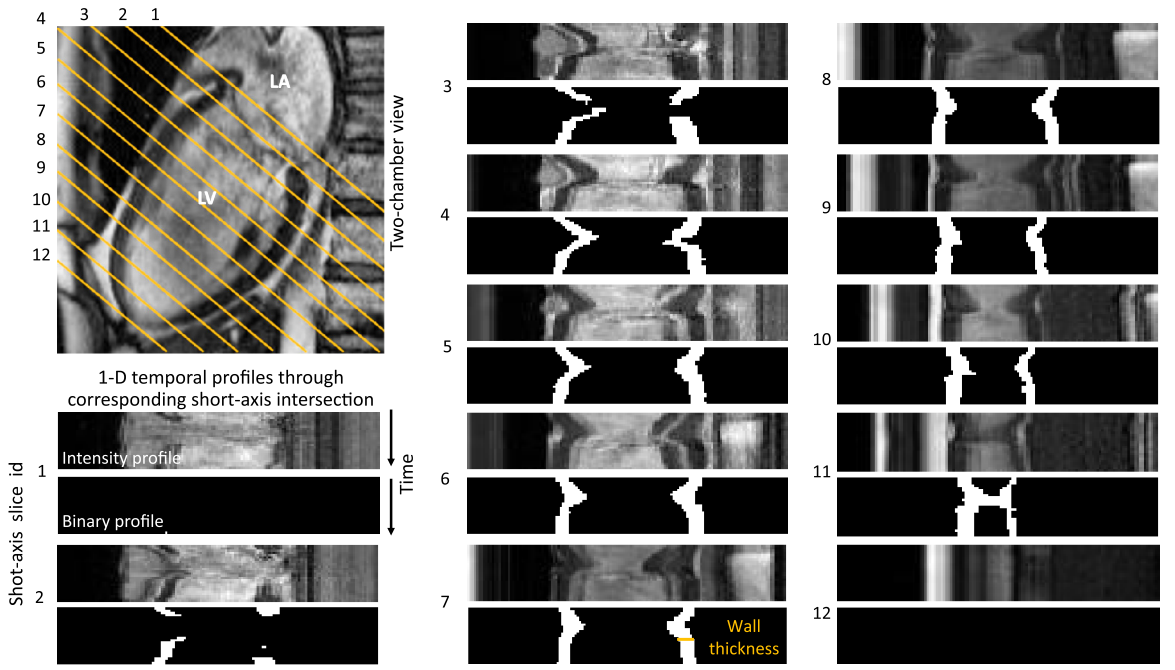

Fig. 5 The two-chamber view intensity and segmented (binary) 1-D profile over time at the intersection of the corresponding short-axis view slice. The basal slice is detected based on this information. LA and LV stand for left atrium and left ventricle, respectively.

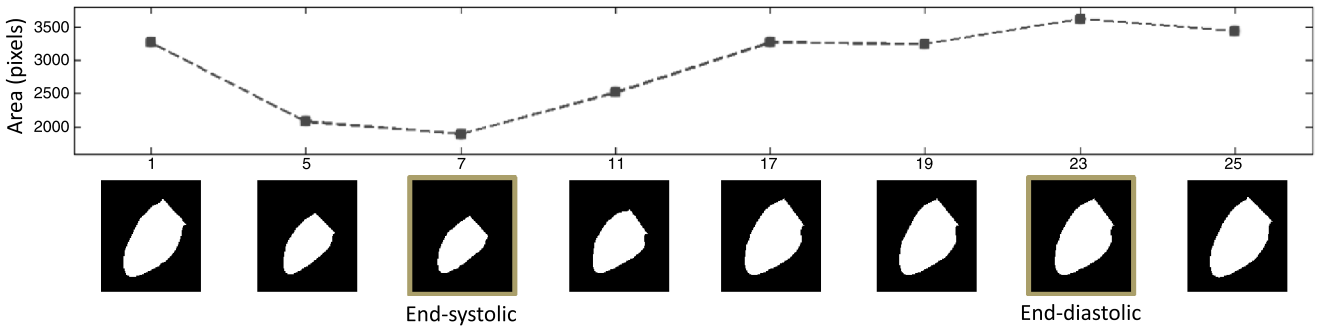

Fig. 6 The end-systolic and end-diastolic phases are estimated by examining the area of the LV in the segmented two-chamber view images. The time of these phases are used to constrain the search for the basal slice in the temporal profiles of the short-axis view slices.

phase. Once the basal slice for the end-diastole is detected, searching for the basal slice for the end-systole begins from the selected end-diastole basal slice to the bottom. For both phases, the first short-axis view slice for which the binary profile contains at least one wall of the LV during the whole time window (around the approximated end-diastolic or end-systolic phases) is considered as the basal slice for the corresponding phase. This is subject to the condition that the average thickness of the observed wall in the time window is larger than a defined threshold, where the threshold is set to 60% of the average thickness of the segmented LV wall for that heart. The threshold is set to avoid selecting a short-axis view slice that slightly touches the base but is not inside the LV.

The described basal slice selection algorithm relies on a good segmentation algorithm. In order to decrease this dependency, a condition was added to the algorithm. Specifically, if the status of a wall alternates between observed and not observed in the time window, the short-axis view slice for that profile still has the potential to be the basal slice only if the frequency of the wall being observed in that time window is more than 60%. However, in this case a higher threshold of 70% is set for the average thickness of the observed wall. In Fig. 7, the binary profile for the basal slices of two different hearts are provided. As can be seen in the binary profile of the second heart at end-systole, the segmentation was found to be inaccurate, and consequently decision making was carried out using the 70% threshold. The generally defined 60% threshold also avoids mistaking the left atrium walls for the LV walls, knowing that the former are thinner than the latter.

3 Results

This study was approved by the National Healthcare Group Domain Specific Review Board. The method was applied to clinical data from 51 cases, including 33 MRI scans of patients with degenerative mitral valve regurgitation acquired on a Siemens 3T Biograph mMR scanner, 13 MRI scans of healthy subjects acquired on a Siemens 3T Magnetom Trio, and 5 MRI scans of patients with ST-segment elevation and myocardial

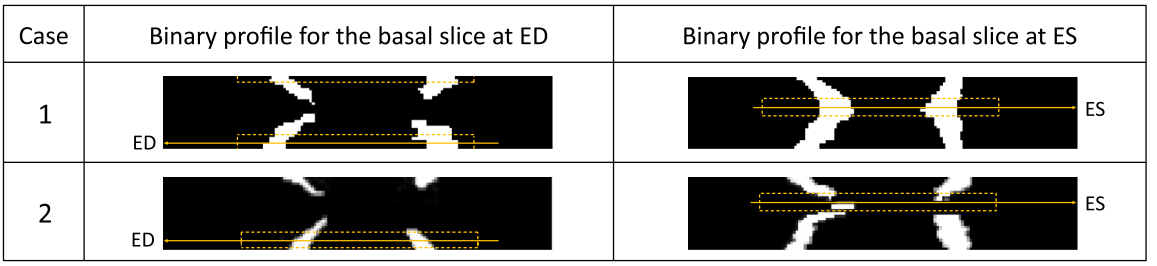

Fig. 7 The 1-D binary profile for the basal slice at the end-diastole and the end-systole for two different hearts. The two profiles in the first row and the first profile in the second row satisfy the 60% threshold rule. The second profile in the second row shows signs of inaccuracy in segmentation, yet it satisfies the 70% threshold rule.

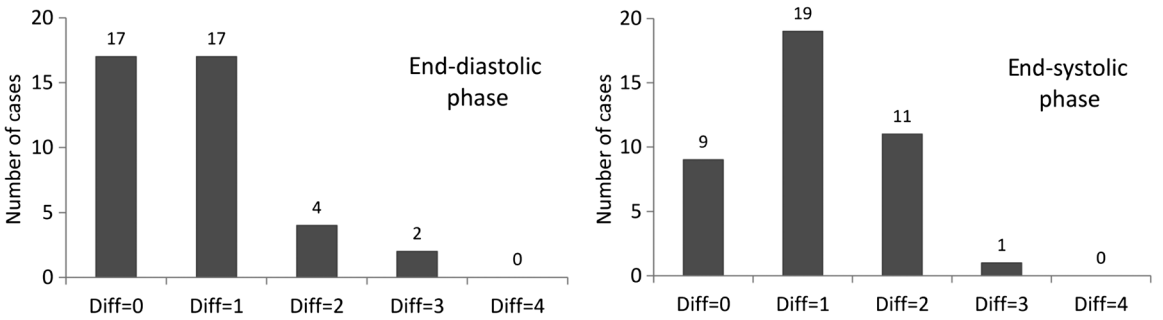

Fig. 8 The number of cases for which 0, 1, 2, 3, or 4 phase-difference was found between the estimated end-diastolic (end-systolic) phase using the two-chamber view slice and the one detected by segmenting the short-axis view slices for the 40 tested hearts.

infarction acquired on a Siemens 3T Magnetom Prisma scanner. Informed consent was obtained from all the subjects. The two-chamber cine CMR sequences comprised of 25 phases and the images were 256×232, 192×192, and 256×216 pixels in size respectively with resolutions in the range of 1.13 to 1.56 mm. Images with 192×192 pixels were upsampled to 256×256 pixels. The short-axis view cine CMR scans included 12 to 15 slices with a similar number of phases. All 25 images of the two-chamber views were segmented by applying the ASM model as described in Sec. 2. The average segmentation error at the basal part of the LV was measured by finding the average vertical distance of the landmarks to the manually segmented LV and was 4.1 mm.

In order to evaluate accuracy of our estimation of the ED and ES phases, the proposed method was applied to manually segmented two-chamber view slice of 40 different hearts from our 51 heart samples and the estimated end-systolic and end-diastolic phases were compared with the same phases identified by segmentation of the short-axis view slices of those hearts. Figure 8 shows the number of cases for which the difference between the two methods was 1, 2, 3, or 4 phases for both the end-diastolic phase (left) and the end-systolic phase (right). Considering the phase differences, a time window of 7 frames was considered while searching for the basal slice.

The basal slice selection algorithm was applied to the series of short-axis view slices for each patient from our 51 heart samples and the results were compared to the manual selections done by an expert prior to this work. For each test case, the basal slice was detected in the end-systolic and the end-diastolic phases, giving a total of 102 basal slices. Overall, the proposed algorithm selects the same basal slices as the expert selection for 47 out of the 51 subjects for end-systole and 43 out of the 51 subjects for end-diastole. We compared the results of our algorithm with those of the proposed method by Tufvesson et al.,[1] which is implemented in the segment tool.[15] Their approach works by segmenting the basal short-axis view slices by considering 24 circumferential sectors over the LV, which are analyzed individually and removed in case no myocardium is detected. We used the segment tool to automatically segment the short-axis view slices of the same test data. The topmost short-axis view slice with more than 50% myocardium segmentation in the end-diastolic phase was defined as the basal slice for end-diastole. The basal slice for end-systole was defined similarly. The results are shown in Table 1. Additionally, the proposed method is compared statistically to the expert's analysis using intraclass correlation coefficient (ICC) in Table 2. As can be seen, our algorithm performs significantly better than the

Table 1 Accuracy of the proposed algorithm for basal slice selection for the end-diastolic phase and the end-systolic phase compared to the segment tool.

	Success rate (ED)	Success rate (ES)
Proposed algorithm	43/51 (84%)	47/51 (92%)
Segment tool	26/51 (51%)	17/51 (33%)

Table 2 ICC for the proposed method and segment tool against the expert's analysis.

ICC	EDV	ESV	EF
Proposed algorithm	0.996	0.971	0.963
Segment tool	0.979	0.761	0.544

segment tool (p-value<0.05). The mean and standard deviation for the measured ED volume, ES volume, and EF by our algorithm, the segment tool, and the expert are also shown in Table 3. The values indicate that the proposed algorithm provides closer measurements to the expert's measurements for all the three parameters. The average running time for our algorithm was about 24 s on a 64-bit machine with 16GB of RAM and Intel Core i7 CPU.

Table 3 Mean and standard deviation of the measured ED volume, ES volume, and EF by the proposed algorithm, the segment tool, and the expert.

Mean ± Std	EDV (ml)	ESV (ml)	EF(%)
Proposed algorithm	146.6 ± 33.3	49.3 ± 14.7	66.1 ± 8.9
Segment tool	136.2 ± 38.3	47.2 ± 16.5	65.2 ± 7.1
Expert's analysis	146.3 ± 33.6	48.9 ± 14.9	66.3 ± 8.9

As previously mentioned, our basal slice selection algorithm failed in a certain number of cases. Table 4 shows details of these failed cases. The second and the third columns show the difference between the selected basal slice by our algorithm and the expert's selection for end-diastole and end-systole, respectively. Also shown are the LV ED volume, ES volume, and EF for the proposed algorithm, the segment tool, and their differences. The mean absolute differences for the measured ED volume, ES volume, and EF are reported in the last row of this table. The mean absolute difference of 4.13% for the EF indicates that in case of failure in basal slice detection, the error in EF measurement by the proposed algorithm still remains in the range of interobserver variability (6%) reported in the literature.

Examples of detection results are shown in Fig. 9. Also shown are the corresponding short-axis view slices, including

Table 4 The difference between the detected basal slice by the proposed algorithm and the expert selected basal slice for ED (second column) and ES (third column). The Ed volume, the ES volume, and the EF are also shown for the detected basal slice by the proposed algorithm and the expert. The last line shows the mean absolute difference and the standard deviation for the measurements.

	Basal diff.		EDV (ml)			ESV (ml)			EF (%)		
Failed cases	ED	ES	Proposed	Expert	Difference	Proposed	Expert	Difference	Proposed	Expert	Difference
1	−1	−1	117.1	126.0	−8.96	34.9	45.4	−10.48	70.2	64.0	6.20
2	−1	0	115.5	123.2	−7.73	37.3	36.8	0.50	67.7	70.1	−2.43
3	−1	0	128.9	140.0	−11.15	36.0	35.7	0.36	72.0	74.5	−2.48
4	1	0	95.0	87.4	7.56	23.7	24.0	−0.27	75.1	72.6	2.47
5	1	0	162.6	150.4	12.23	46.2	46.6	−0.41	71.6	69.0	2.58
6	1	1	107.1	101.1	6.03	38.4	29.5	8.90	64.1	70.8	−6.66
7	1	1	117.4	110.1	7.23	36.2	29.8	6.42	69.1	73.0	−3.80
8	1	1	131.3	121.5	9.81	56.2	44.2	11.96	57.2	63.6	−6.39
Mean absolute error ± Std					8.84 ± 2.11			4.91 ± 5.08			4.13 ± 1.95

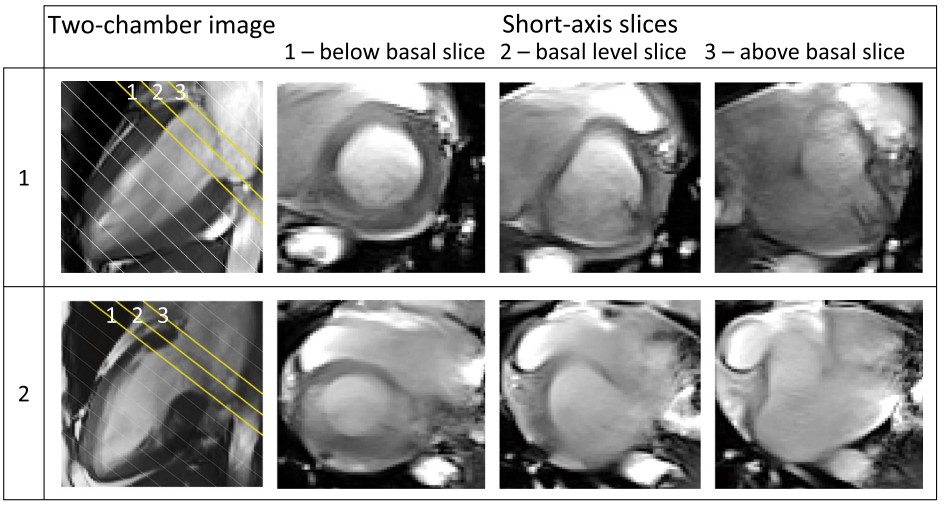

Fig. 9 Two examples of correctly identified basal slices (middle). The figure also shows adjacent slices to the basal slice, the left slice is the next slice inside the LV, and the right slice is out of the LV.

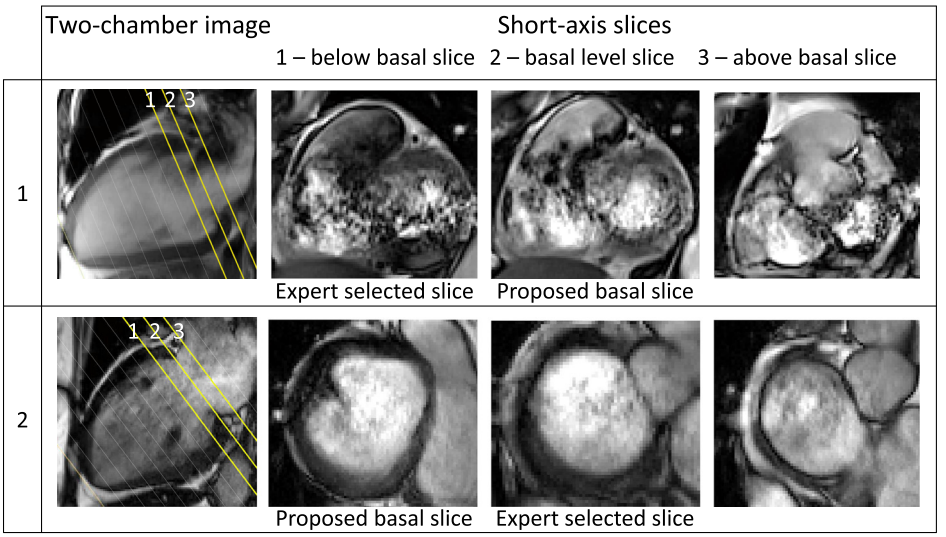

Fig. 10 Two examples of segmentation results that were different from the expert selected basal slice. In the first case, an incorrect slice was selected as the basal slice by the expert. In the second case, an incorrect slice was selected as the basal slice by the proposed algorithm.

the slice below the basal slice (left), the basal slice (middle), and the slice above the basal slice (right). These additional slices are included to reveal the complexity of the basal slice appearance in the short-axis view images. For both cases the proposed algorithm selected the same basal slice as the expert. One can see that selecting the short-axis view slice below the line that connects the mitral valve points would give incorrect results for the first case. It is worth mentioning that we found 10 cases in the 51 MRI scans for which the previous definition did not provide a correct basal slice.

Figure 10 shows two examples for which the proposed algorithm selected a different slice in the end-diastolic phase than manual selection. Regarding the first case, the short-axis view image for this slice is of poor quality due to significant artifacts caused by blood movement around this area and consequently prevents the expert from making a good judgment about the correct basal slice. However, the basal slice for this case can be found by looking at the two-chamber view. The second example highlights the importance of having a correct segmentation algorithm. Wrong selection in this case stems from the fact that the basal slice is almost tangent to the base of the LV and consequently a minor error in segmentation of this area on the two-chamber view can prevent correct selection of the basal slice.

4 Discussion

An automatic basal slice selection algorithm is proposed using the two-chamber view of the LV. The end-systolic and end-diastolic phases are estimated using the same view. As a result, the algorithm can be incorporated into any software and selection of the basal slice can be carried out at the loading of the image sequences without the need for manual interaction. The proposed method follows the SCMR guidelines for basal slice selection.

With regards to the current performance of landmark detection algorithms,[8,9] updating these methods to the SCMR guidelines may not result in as accurate a basal slice detection algorithm as the proposed method in this paper. Further improvement is needed for this class of methods to be able to utilize them for our purpose. Not having a basic shape from the two-chamber view, the myocardium needs to be segmented using a method that values the morphology as importantly as the intensity, texture, and contextual information. ASM[14] is an excellent example of such a method. This method allows us to estimate the percentage of myocardium around the blood cavity by examining the two-chamber view slice and finding the thickness of both walls of LV in this slice. Other methods such as AAMs[16] or 3-D models[12,13] have also been introduced previously. However, these methods are usually slower and cannot provide fast results for the problem being discussed in this paper. The proposed algorithm performs better than the state-of-the-art method[1] for basal slice selection. The poor performance of this existing method[1] mainly stems from the low quality of short-axis view slices in the base, which makes myocardium segmentation difficult and also explains the poor interobserver reproducibility in manual selection of the basal slice.[6,7]

Collecting the thickness of the two walls for the basal slice for all the patients in the training dataset showed that at least one of the walls should be more than 60% as thick as the average thickness of myocardium in order to consider this short-axis view slice inside the LV. The 70% threshold set for the cases with high segmentation error was defined empirically. The proposed algorithm is a reliable strategy for automation of the basal slice, which can reduce the intra- and interobserver variabilities in medical reports for a more consistent diagnostic or medical trial. This is mainly because the proposed method does not require any user input and therefore is fully automatic. As a result, there is no interobserver variability impact on basal slice selection. The only remaining reproducibility errors result from segmentation of the short-axis view slices, which are a similar problem for the segment tool or manual segmentation.

Although the two-chamber view provides an overview of two opposite walls of LV that are very close to the center of the ring, the authors agree that making decisions based on the information obtained from this view is not physically equivalent to the 50% myocardium rule. A more accurate estimation would be to use the four-chamber view as well.

5 Conclusion

A framework for automatic basal slice detection that follows the SCMR guidelines is presented. The key idea of the approach is to examine the status of the segmented two-chamber ventricle walls that pass through the short-axis view slices. It was also shown that the two-chamber view can be used to provide a good estimation of the end-systolic and the end-diastolic phases and consequently, it does not require any segmentation of the short-axis view slices. The method produces results in accordance with manually selected basal slices for normal and diseased hearts. Future work will use the information from the short-axis view for validation of the two-chamber view segmentation results and will perform the basal slice selection for every time frame of the cardiac cycle for a complete four-dimensional function evaluation.

Acknowledgments

This work has been partially funded by the Singapore NMRC NUHS Centre Grant – Medical Image Analysis Core (NMRC/CG/013/2013). The authors declare that they have no conflicts of interest or financial interests.

References

1. J. Tufvesson et al., "Validation and development of a new automatic algorithm for time-resolved segmentation of the left ventricle in magnetic resonance imaging," *BioMed Res. Int.* **2015**, 970357 (2015).
2. I. B. Ayed et al., "Left ventricle segmentation via graph cut distribution matching," in *Medical Image Computing and Computer-Assisted Intervention (MICCAI)*, Vol. **5762**, pp. 901–909, Springer (2009).
3. M. P. Jolly et al., "Combining registration and minimum surfaces for the segmentation of the left ventricle in cardiac cine MR images," in *Medical Image Computing and Computer-Assisted Intervention (MICCAI)*, Vol. **5762**, pp. 910–918, Springer (2009).
4. C. Petitjean and J. N. Dacher, "A review of segmentation methods in short axis cardiac MR images," *Med. Image Anal.* **15**(2), 169–184 (2011).
5. A. Suinesiaputra et al., "Left ventricular segmentation challenge from cardiac MRI: a collation study," in *Statistical Atlases and Computational Models of the Heart, Imaging and Modelling Challenge*, Vol. **7085**, pp. 88–97, Springer (2012).
6. J. T. Marcus et al., "The influence of through-plane motion on left ventricular volumes measured by magnetic resonance imaging: implications for image acquisition and analysis," *J. Cardiovasc. Magn. Reson.* **1**(1), 1–6 (1999).
7. S. Marchesseau, J. X. Ho, and J. J. Totman, "Influence of the short-axis cine acquisition protocol on the cardiac function evaluation: a reproducibility study," *Eur. J. Radiol.* **3**, 60–66 (2016).
8. D. Mahapatra, "Landmark detection in cardiac MRI using learned local image statistics," in *Statistical Atlases and Computational Models of the Heart, Imaging and Modelling Challenges*, Vol. 7746, pp. 115–124, Springer (2013).
9. X. Lu and M. P. Jolly, "Discriminative context modeling using auxiliary markers for LV landmark detection from a single MR image," in *Statistical Atlases and Computational Models of the Heart, Imaging and Modelling Challenges*, Vol. **7746**, pp. 105–114, Springer (2013).
10. J. Schulz-Menger et al., "Standardized image interpretation and post processing in cardiovascular magnetic resonance: society for cardiovascular magnetic resonance (SCMR)," *J. Cardiovasc. Magn. Reson.* **15**(35), 1167–1186 (2013).
11. M. Uzumcu et al., "Multiview active appearance models for simultaneous segmentation of cardiac 2- and 4-chamber long-axis magnetic resonance images," *Invest. Radiol.* **40**(4), 195–203 (2005).
12. X. Zhuang et al., "A registration-based propagation framework for automatic whole heart segmentation of cardiac MRI," *IEEE Trans. Med. Imaging* **29**(9), 1612–1625 (2010).
13. H. C. V. Assen et al., "SPASM: a 3D-ASM for segmentation of sparse and arbitrarily oriented cardiac MRI data," *Med. Image Anal.* **10**(2), 286–303 (2006).
14. T. F. Cootes et al., "Active shape models—their training and application," *Comput. Vision Image Understanding* **61**(1), 38–59 (1995).
15. E. Heiberg et al., "Design and validation of segment a freely available software for cardiovascular image analysis," *BMC Med. Imaging* **10**(1), 1 (2010).
16. T. F. Cootes et al., "Active appearance models," *IEEE Trans. Pattern Anal. Mach. Intell.* **23**(6), 681–685 (2001).

Mahsa Paknezhad is a PhD student at the National University of Singapore. She received her BS and MS degrees in information technology engineering from Shiraz University of Technology in 2011 and 2013, respectively. Her research focuses on using computer vision and image processing to solve problems in the area of medical image analysis. Recently, she has taken an active interest in cardiac image analysis.

Stephanie Marchesseau obtained an engineering degree from "Ecole des Mines de Nancy" (France), and a MSc degree of applied maths and theoretical physics from the University of Cambridge (UK) in 2008. She obtained her PhD from "Ecole des Mines de Paris" (France) in 2013 for her work at Inria Sophia Antipolis (France). From January 2013, she pursued her postdoctoral research at Asclepios. Since March 2014, she has been a research fellow at Clinical Imaging Research Center.

Michael S. Brown is a professor in the Department of Electrical Engineering and Computer Science at York University. His research interests include computer vision, image processing, and computer graphics. He is currently an associate editor for the *IEEE Transactions on Pattern Analysis and Machine Intelligence* and the *International Journal of Computer Vision*.